doi:10.1038/nature11601

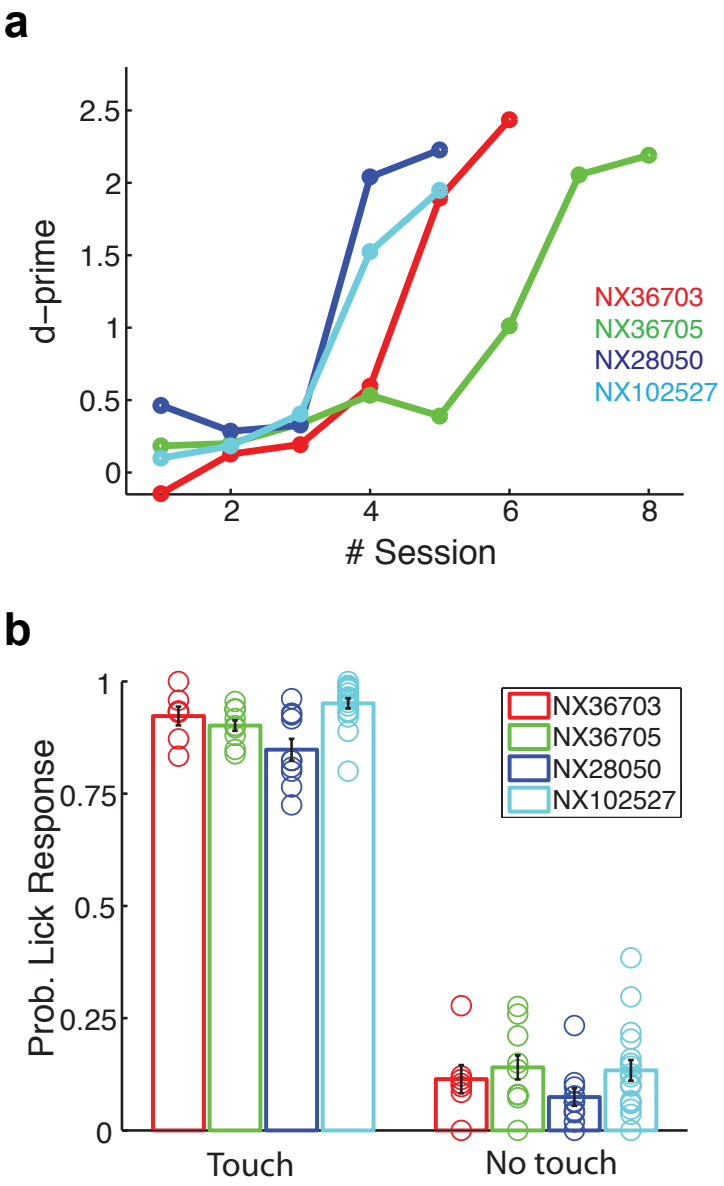

Supplementary Figure 1 | Behavioral performance before and during the start of imaging sessions. **a,** Behavioral performance of the tactile detection task measured by *d'* (see Methods) during training period. Colors indicates the 4 animals used in the current study. Imaging session began typically after *d'* reached >1.5 (typically > 75% of overall correct). **b,** Behavioral response during imaging session measured by percent of trials with lick response in trials with (Touch) and without (No touch) whisker-object contact, as determined from high speed videography.

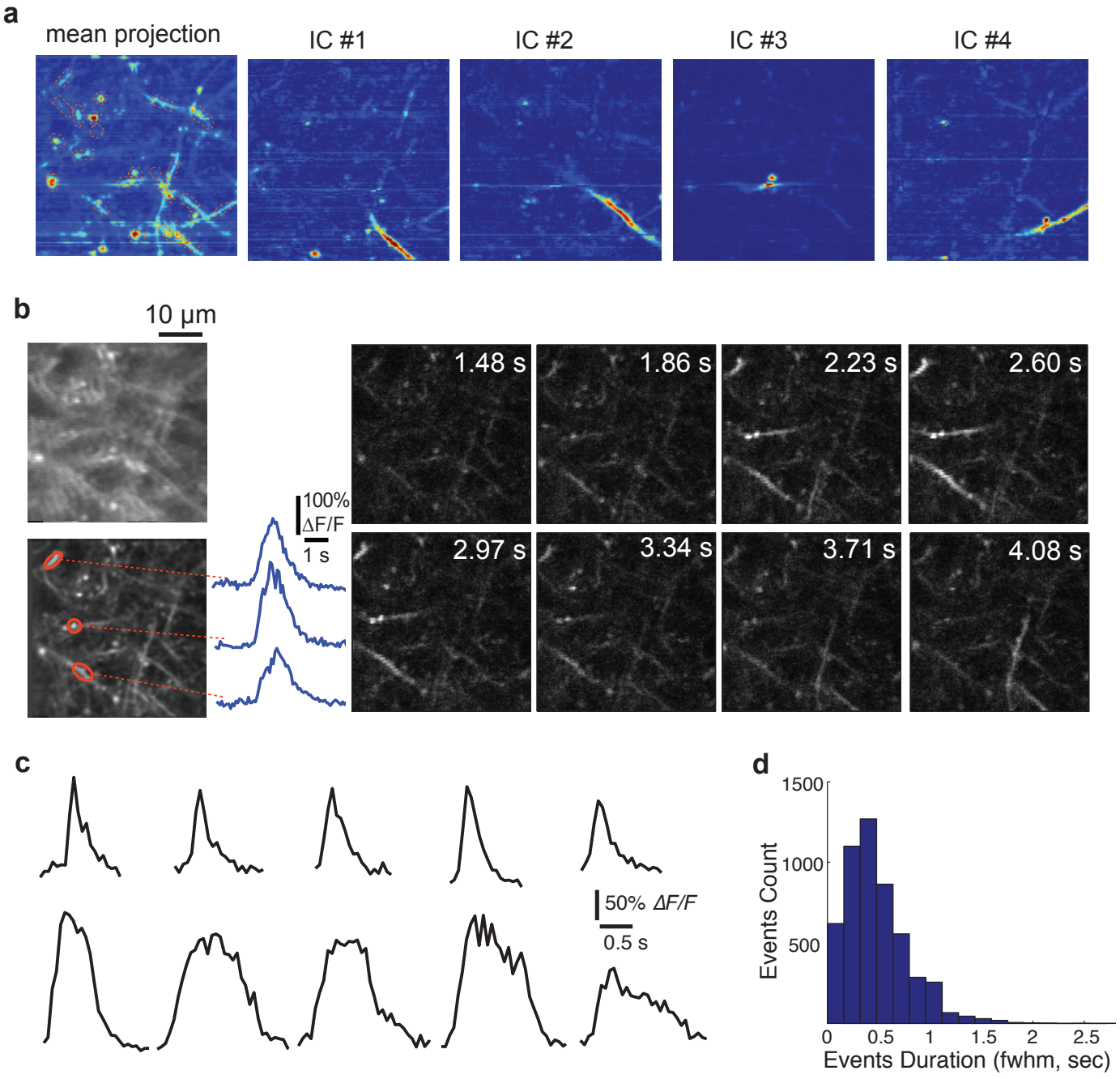

Supplementary Figure 2 | ICA based ROI selection and dendritic Ca^{2+} signals. **a,** Example of independent components showing "hot spots" of spatially and temporally more independent pixels that match underlying dendritic structures. ROIs were manually selected based on ICA hot spots and two-photon images. Overlapping of ROIs was avoided based on the mean projection of all ICA images. **b,** Motion correlction and example Ca^{2+} signal. Left, Mean projection of 100 two-photon imaging frames from a single behavioral trial before (upper) and after (lower) motion correction using a combination of whole frame image registration and line-by-line registration. The motion artifacts due to animal movement are largely removed. Right, extracted fluorescence time series from identified ROIs (labeled by red lines) and example two-photon imaing frames. **c,** Example traces of dendritic Ca^{2+} transients during behavior showing both simple (upper row) and complex (bottom row) kinetics. **d**, Distribution of duration of calcium events during behavioral sessions.

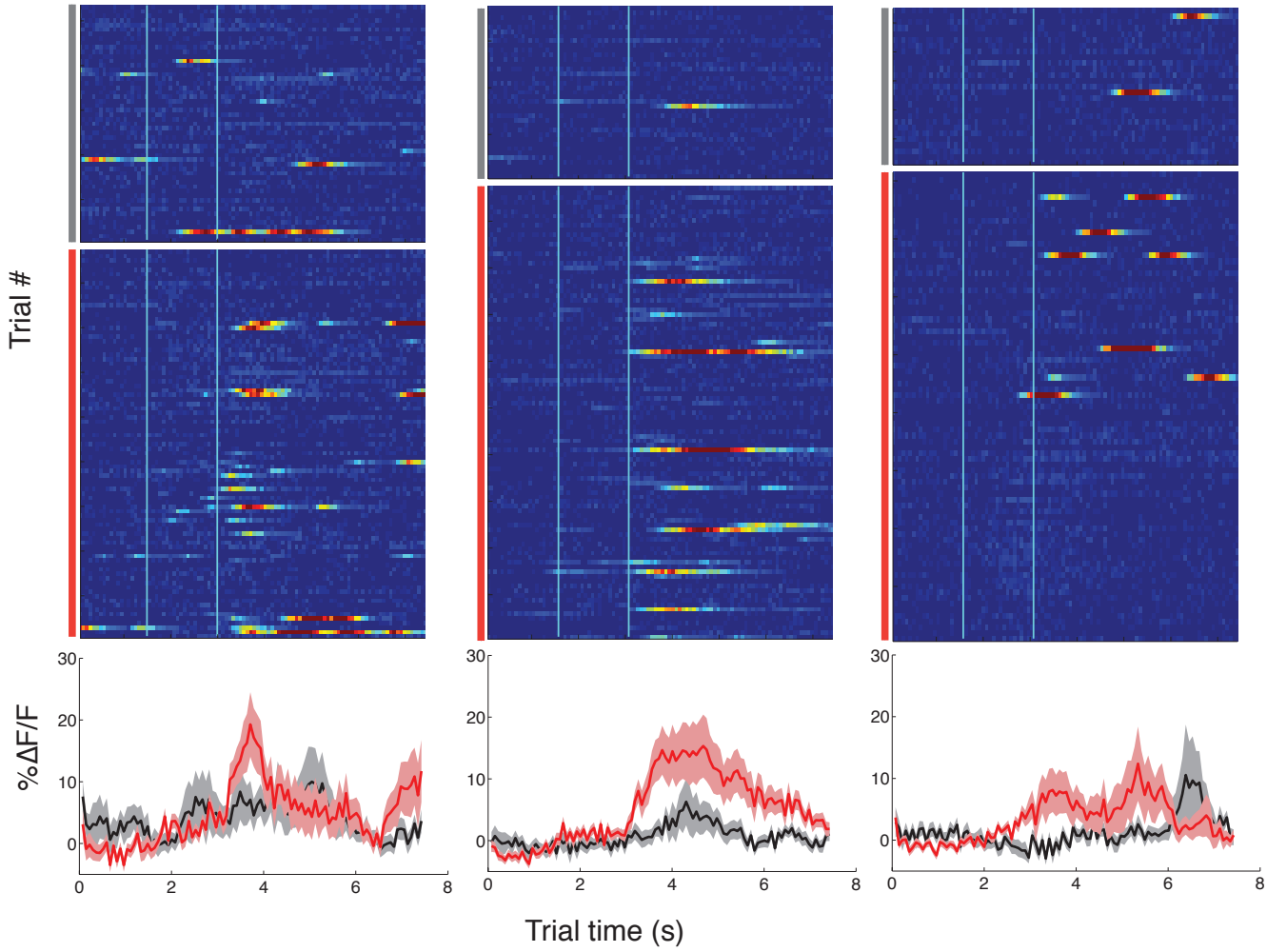

Supplementary Figure 3 | Example dendritic ROIs showing less reliable response outside whisker sampling epoch. Upper panels, color raster plot of Ca^{2+} signal ($\Delta F/F$) from 3 example dendritic ROIs 3 experiments. Each row of pixels depicts a trial. The group of trials containing whisker-object contact (indicated by the red bar on the left) are separate from trials without detectable whisker-object contact (gray bar on the left). Trials within each group are arranged by temporal order with early trials at the bottom. Lower panels, averaged dendritic Ca^{2+} signal (mean ± s.e.m.) trials containing whisker contacts (red), and trials with no contacts (black).

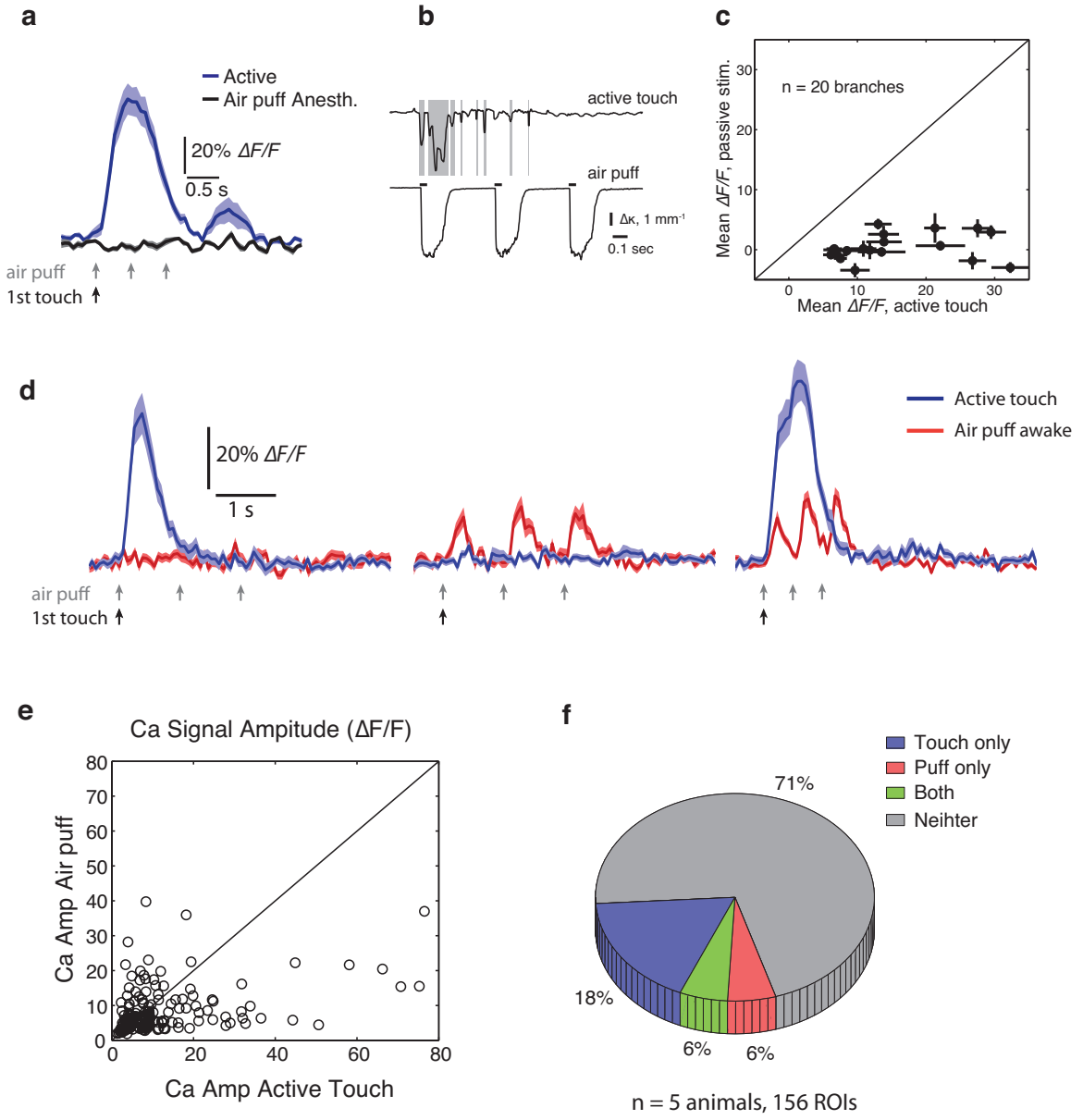

Supplementary Figure 4 | Passive stimulation under awake and anesthetized conditions. **a**, Ca^{2+} signals (mean ± s.e.m.) from an example dendritic branch during behavior with active touch with C2 whisker (aligned to touch onset, black arrow) and during anesthesia with air puff stimulation to the same whisker (aligned to the onset of air puff, 3 pulses, gray arrows). **b,** Whisker curvature change induced by active touch (top trace), and by air puff (bottom trace). **c,** Summary of population data of averaged Ca^{2+} signals from the same dendritic branches during behavior with active touch and during anesthesia with air puff stimuli. Passive stimulation during

anesthesia is ineffective in evoking Ca^{2+} signals from dendrites that were otherwise active during active touch. **d-f,** Dendritic Ca^{2+} signals evoked by air puff to awake mice and by active touch during behavior. **d,** Ca^{2+} signals (mean ± s.e.m.) from a dendritic branch showing responses to active touch but not to air puff (left), a dendritic branch showing responses to air puff but not to active touch (middle), and a dendritic branch showing responses to both air puff and active touch. **e,** Comparing Ca^{2+} signals in response to air puff and active touch for all dendritic ROIs (n = 156 ROIs, 5 animals). Dendrites often show distinct response to air puff and active touch. **f,** The fraction of dendritic ROIs responding to active touch and air puff during awake state. Note that data were only from imaging fields containing active dendritic ROIs responding to active touch, and there were potential cases where more than one ROIs were from the same cell, therefore the total fraction of responsive dendritic ROIs is likely an overestimation.

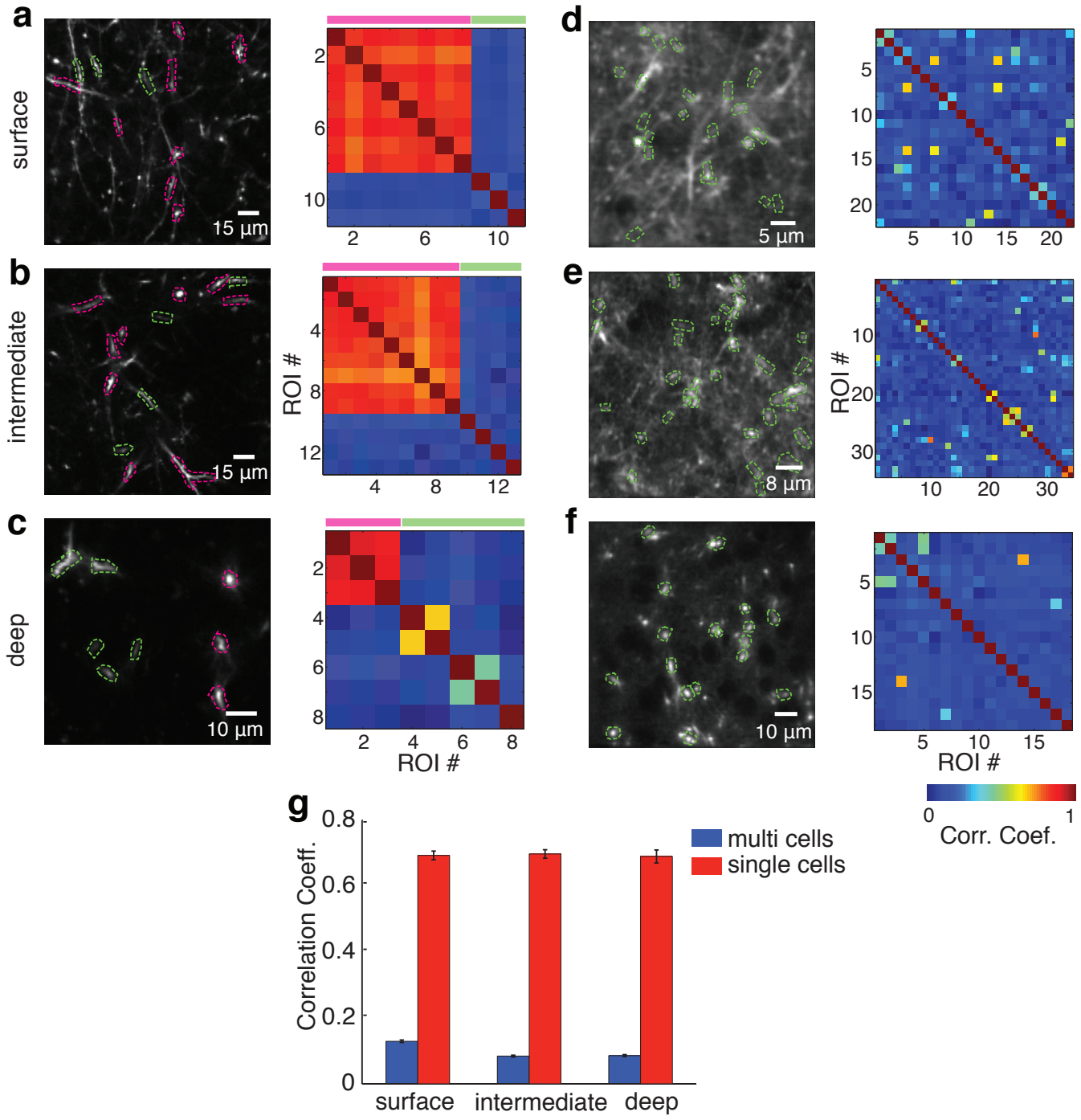

Supplementary Figure 5 | Pair wise correlation for dendritic ROIs imaged at different depth. a-c, Sparse labeling condition [~20 µm in **a**, ~50 µm in **b** ~120 µm in **c**]. Left, two-photon images with active dendritic ROIs labeled with dashed lines. Right, Color maps of correlation coefficient matrices for ROIs shown on the left. Magenta, dendritic ROIs from the same cell. Light green dendritic not traceable to a single apical trunk. **d-f,** Dense labeling condition [~25 µm in **d**, ~46 µm in **e**, ~150 µm in **f**], similarly presented as in **a-c**. **g,** Summary for data shown in **a-f**. Densely labeled (multi cells) and sparsely labeled (single cells) imaging fields were grouped into 3 focal depth ranges (surface, 15-40 µm, R = 0.13 ± 0.14, n = 10 for dense labeling, R = 0.69 ± 0.13, n = 15 for sparse labeling; intermediate branching points, 45-80 µm, R = 0.084 ± 0.13, n = 10 for dense labeling, R = 0.70 ± 0.13, n = 23 for sparse labeling; deep primary branches, 120-200 µm, R = 0.085 ± 0.11, n = 10 for dense labeling, R = 0.69 ± 0.11, n = 9 for sparse labeling).

a

Table1: Paired and unpaired dendritic plateau properties

Preparation (condition)	Amplitude (mV)	Duration (ms)
Anesth. (unpaired tuft)	30.6 ± 0.6	21.2 ± 1.1
Anesth. (paired tuft)	54.2 ± 0.8	68.2 ± 2.6
Slice (unpaired tuft)	45.2 ± 2.4	21.8 ± 0.9
Slice (paired tuft)	66.4 ± 3.7	55.4 ± 5.2
Slice (unpaired trunk)	69.2 ± 1.4	21.2 ± 1.1
Slice (paired trunk)	71.9 ± 3.3	45.8 ± 6.5

Anesthetized unpaired: 38 events from 6 cells, Anesthetized paired: 69 events from 6 cells, Slice: 78 events from 13 cells.

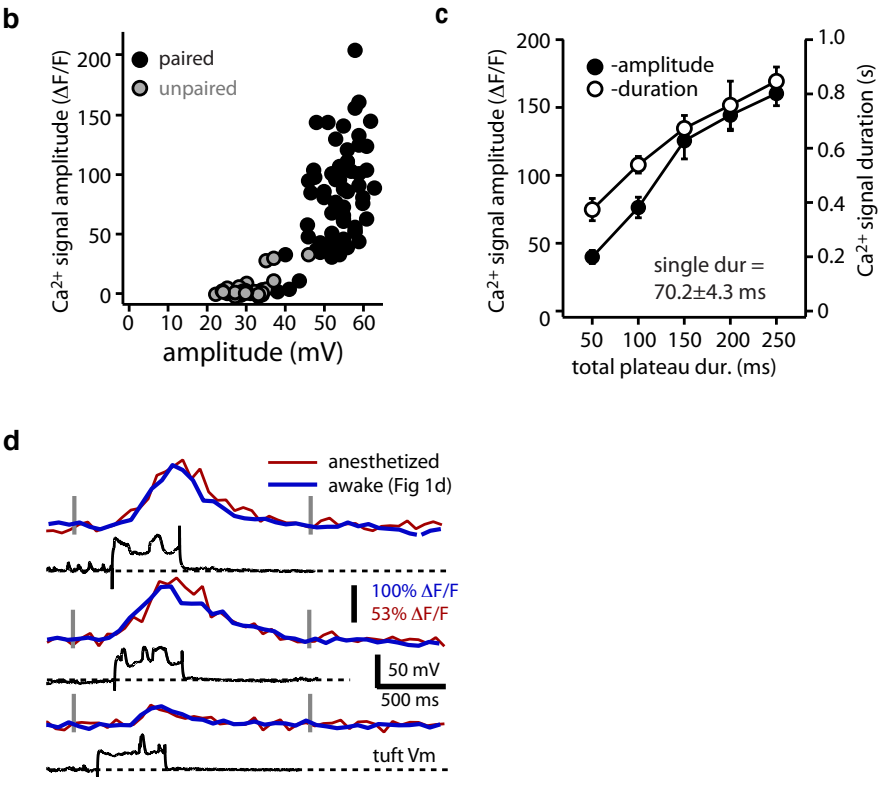

Supplementary Figure 6 | Tuft plateau potential properties. a, Table comparing plateau potential properties across recording conditions. **b,** For recordings from anesthetized mice, Ca^{2+} signal amplitude coarsely varied as a function of local tuft event amplitude. Paired events were larger in amplitude than unparied events and were associated with larger Ca^{2+} signals. **c,** Ca^{2+} signal amplitude and duration as a function of total duration of plateau potentials from simultaneous in vivo imaging and voltage recordings. **d,** Ca^{2+} and voltage traces from an anesthetized mouse (red traces) show that multiple plateau potentials enhance the amplitude and duration of the Ca^{2+} signals. These traces are superimposed by Ca^{2+} signals recorded from behaving mice (blue; gray lines indicate sampling period; traces from Fig. 1d).

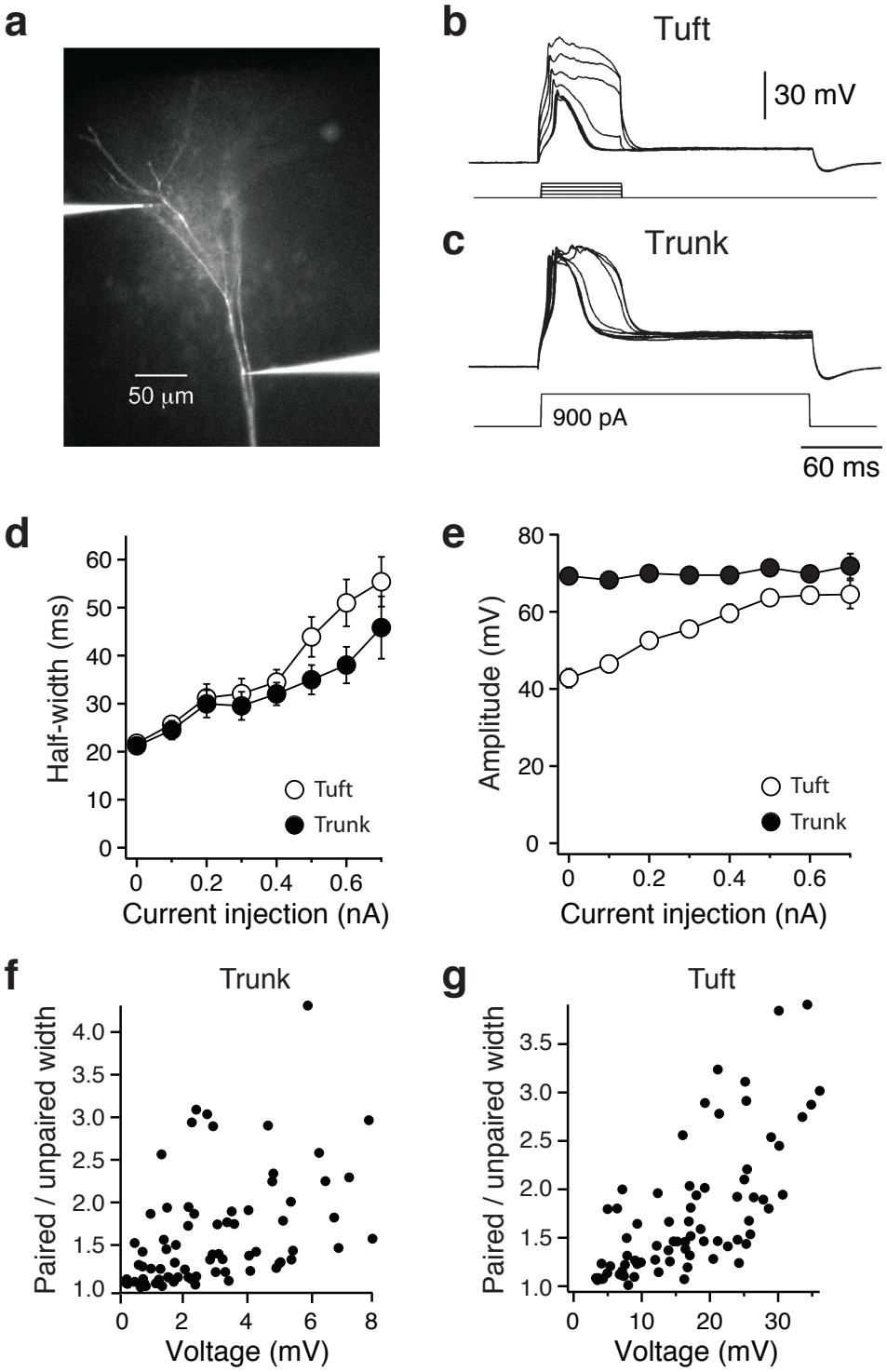

Supplementary figure 7 | Simultaneousual dual whole-cell voltage recordings from the distal apical trunk and tuft regions of a L5 pyramidal neuron. a, Wide-field fluorescent image of recordings (trunk at 700 um; tuft at 900 um). **b,** Back-spread of trunk spike into tuft paired with local current injections ranging from 0-600 pA (60 ms). **c,** Trunk spikes evoked by 900 pA injection (20 ms). **d,** Trunk spike and tuft plateau potential durations or (**e**) amplitudes versus local current injection amplitude. **f,** Increase in trunk spike or (**g**) tuft plateau potential durations as a function of depolarization.

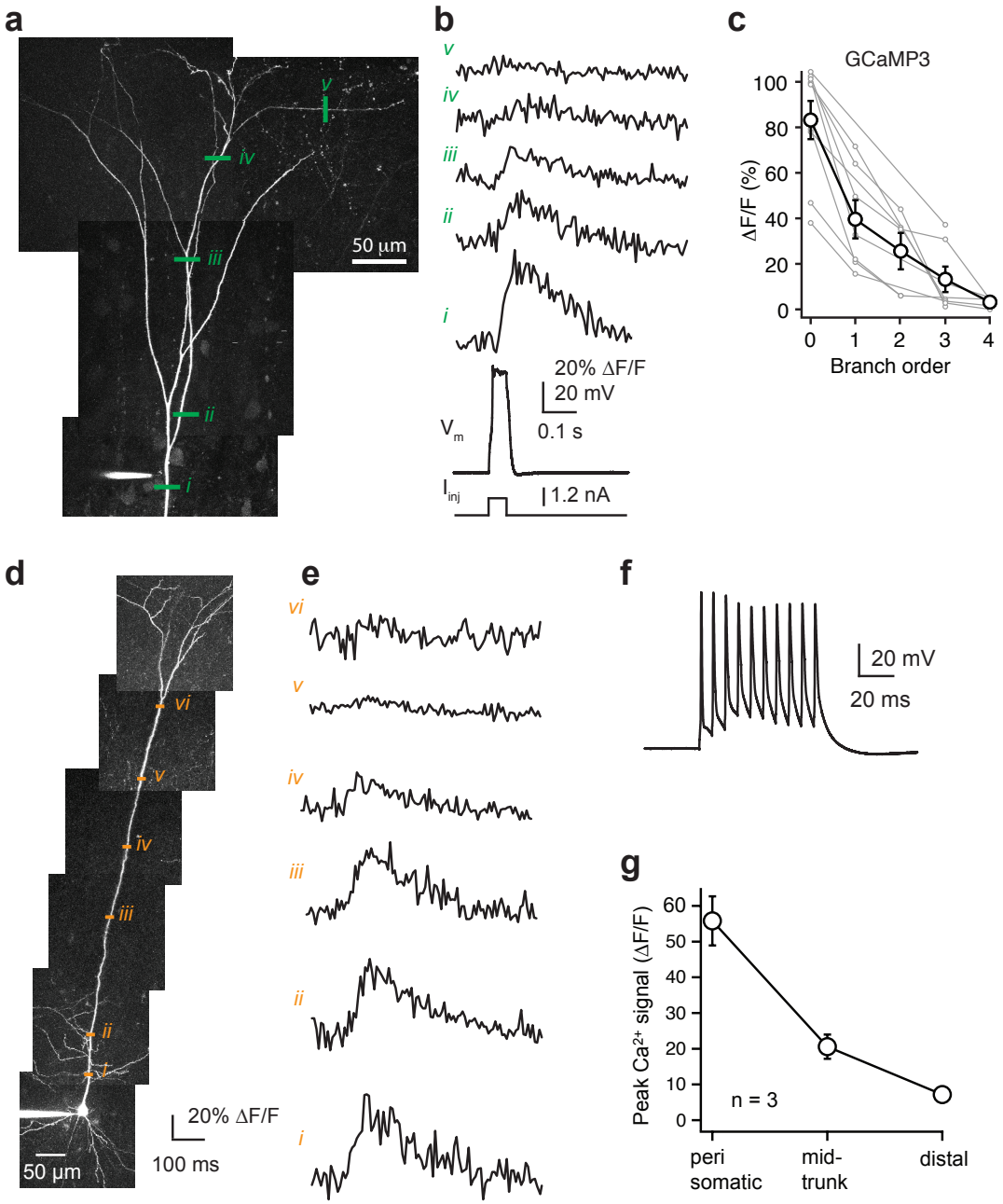

Supplementary Figure 8 | Plateau potentials and back-propagating action potentials are not sufficient to generate tuft Ca^{2+} transients. **a,** Maximal z-projection of an example GCaMP3(+) rat L5 pyramidal neuron apical tuft in an acute slice indicating electrical and optical recording locations. **b,** GCaMP3 signals in response to plateau potentials evoked by nexus current injection (bottom) along apical tuft dendrites (top). **c,** Summary of plateau potential-evoked GCaMP3 signals in the distal apical arbor of L5 pyramids (n = 9 cells and 42 branches). **d,** Z-stack image of a GCaMP3(+) positive L5 pyramidal neuron patched at the soma. Line-scan two-photon imaging of CaMP3 as performed at different distances along the apical dendrite from the soma indicated by the orange bars and numerals. **e,** Average two-photon fluorescence traces recorded from the dendritic locations indicated in (**d**) in response to a train of high frequency somatic action potentials at the soma as shown in (**f**). **f**, Voltage recording of a train of high frequency action potentials from the soma of the neuron shown in **d-e**, evoked by somatic current injection. **g,** Grouped data summarizing the attenuation of Ca^{2+} signal recorded from apical dendrites with increasing distance from soma in response to high frequency somatic action potentials by current injection.

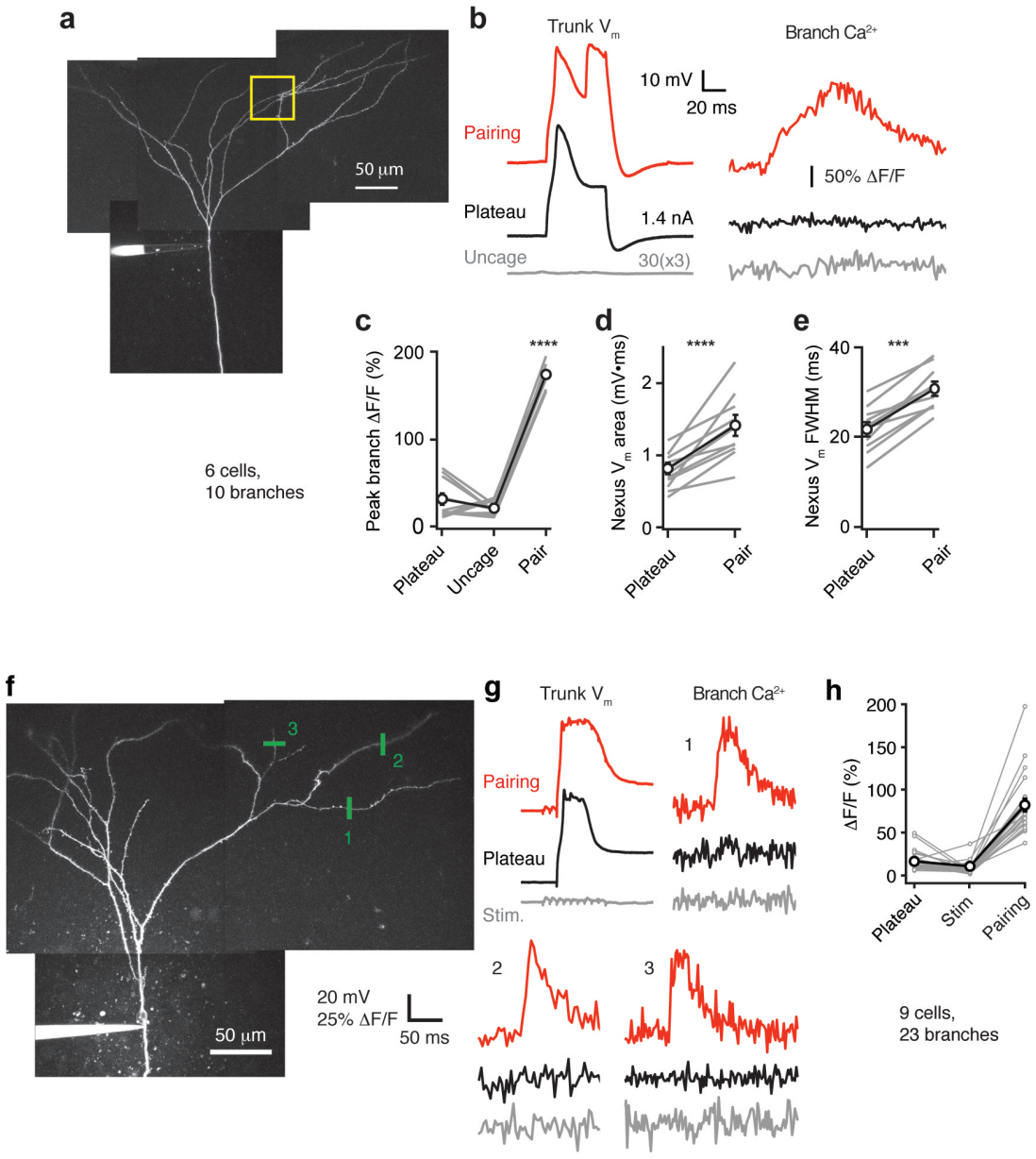

Supplementary Figure 9 | Distal synaptic input rescues plateau potential backpropagation in L5 tuft dendrites in acute brain slices. a, Maximal two-photon z-projection of a L5 pyramidal neuron tuft patched near the nexus illustrating two-photon linescan locations (numbered green bars). **b,** Voltage traces recorded at the nexus (top left) and associated local OGB-6F signals recorded at the three branches of interest indicated in (**a**) (top right and bottom) in response to nexus current injection alone (1.0 nA, just above threshold for plateau potential generation; black traces), synaptic stimulation alone (10 pulses of 0.2 ms at 100 Hz delivered via a bipolar stimulating electrode placed ~50-100 μm from the dendrites of interest; grey traces) and pairing these two paradigms (current injection delayed by 25 ms relative to the synaptic stimulation; red traces). **c,** Summary of tuft branch OGB-6F signals in 23 branches assessed in 9 neurons where distal synaptic stimulation was paired with nexus current injection (pairing significantly greater than either plateau or synaptic stimulation alone: $p<0.0001$, one-way repeated measures ANOVA). **d,** Z-stack of a L5 neuron tuft patched at the nexus with two-photon glutamate uncaging and imaging location highlighted by the yellow box. **e,** Voltage recorded at the nexus (left) and local branch OGB-6F signals (right) in response to current injection at the nexus (1.4 nA, just above threshold; black traces), prolonged subthreshold uncaging at the branch of interest (30 points, cycled 3 times, 1.0 ms isi; grey traces), and pairing (uncaging leading current injection by 20 ms; red traces). **f,** Summary of tuft branch OGB-6F signals from 10 branches in 6 neurons where nexus current injection was paired with prolonged, subthreshold uncaging (pairing significantly greater than either plateau or uncaging alone: $p<0.0001$, one-way repeated measures ANOVA). **g,** Pairing significantly increased plateau potential area ($p<0.0001$, paired t-test) and h, full width at half maximal amplitude ($p=0.0006$, paired t-test).

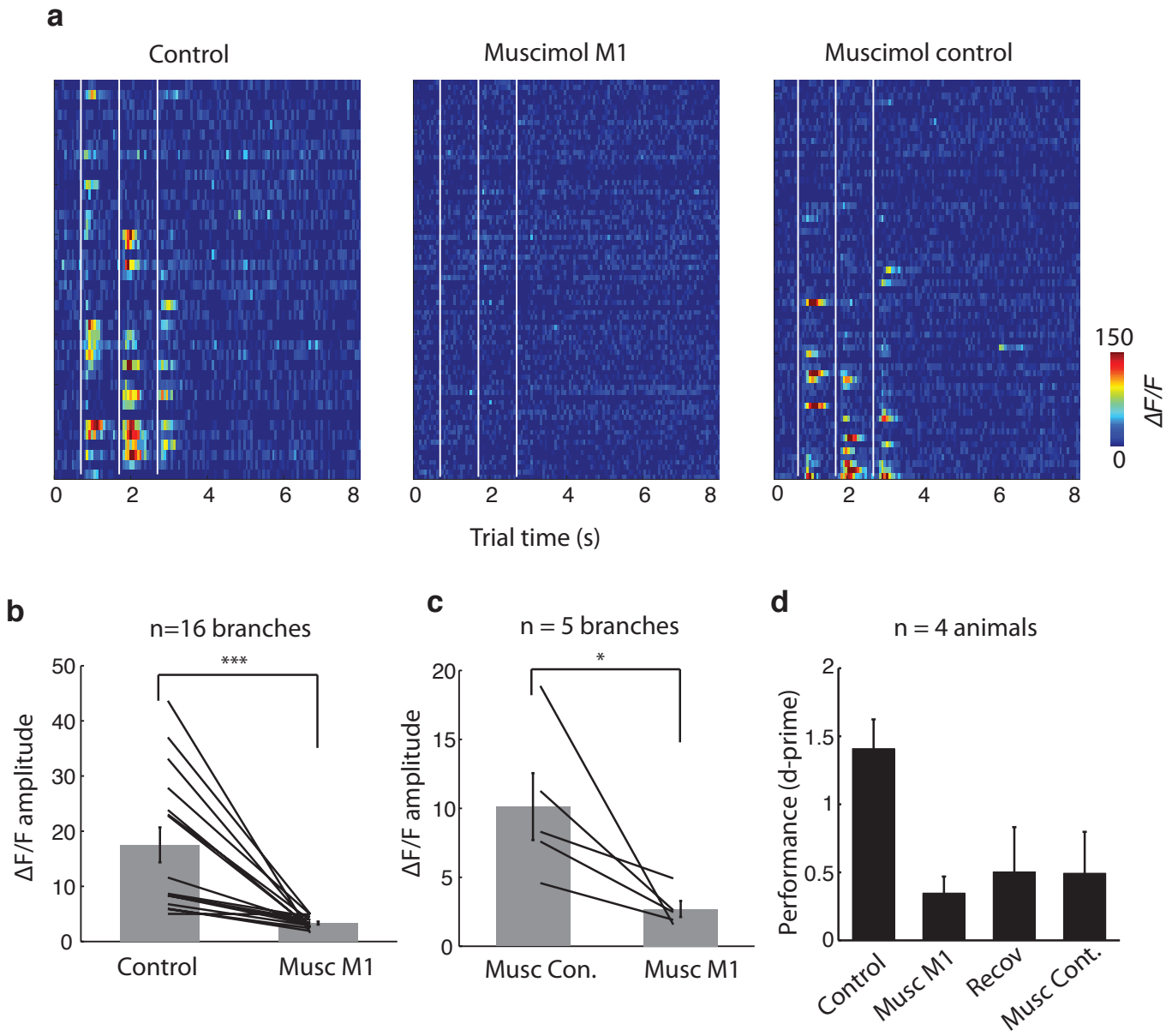

Supplementary Figure 10 | Effects of M1 silencing on air puff evoked responses and behavioral performance. **a,** Color raster plot of Ca^{2+} signals from air puff trials under awake state during control session (left), during a session with muscimol injected to M1 (middle), and with muscimol injected to the control site (right). **b,** Summarized data comparing Ca^{2+} signals (averaged from all trials for each dendritic ROI) from dendritic branches imaged during control sessions and sessions with muscimol injected to M1. **c,** Summarized data comparing Ca^{2+} signals from dendritic branches imaged during sessions with muscimol injected to M1, and to the control site. **d,** Behavioral performance (d-prime) under different conditions in consecutive sessions. Note that task performance was strongly suppressed by M1 inactivation, and did not recover to control level in the following sessions, suggesting an unlearning process occurred during M1 inactivation.

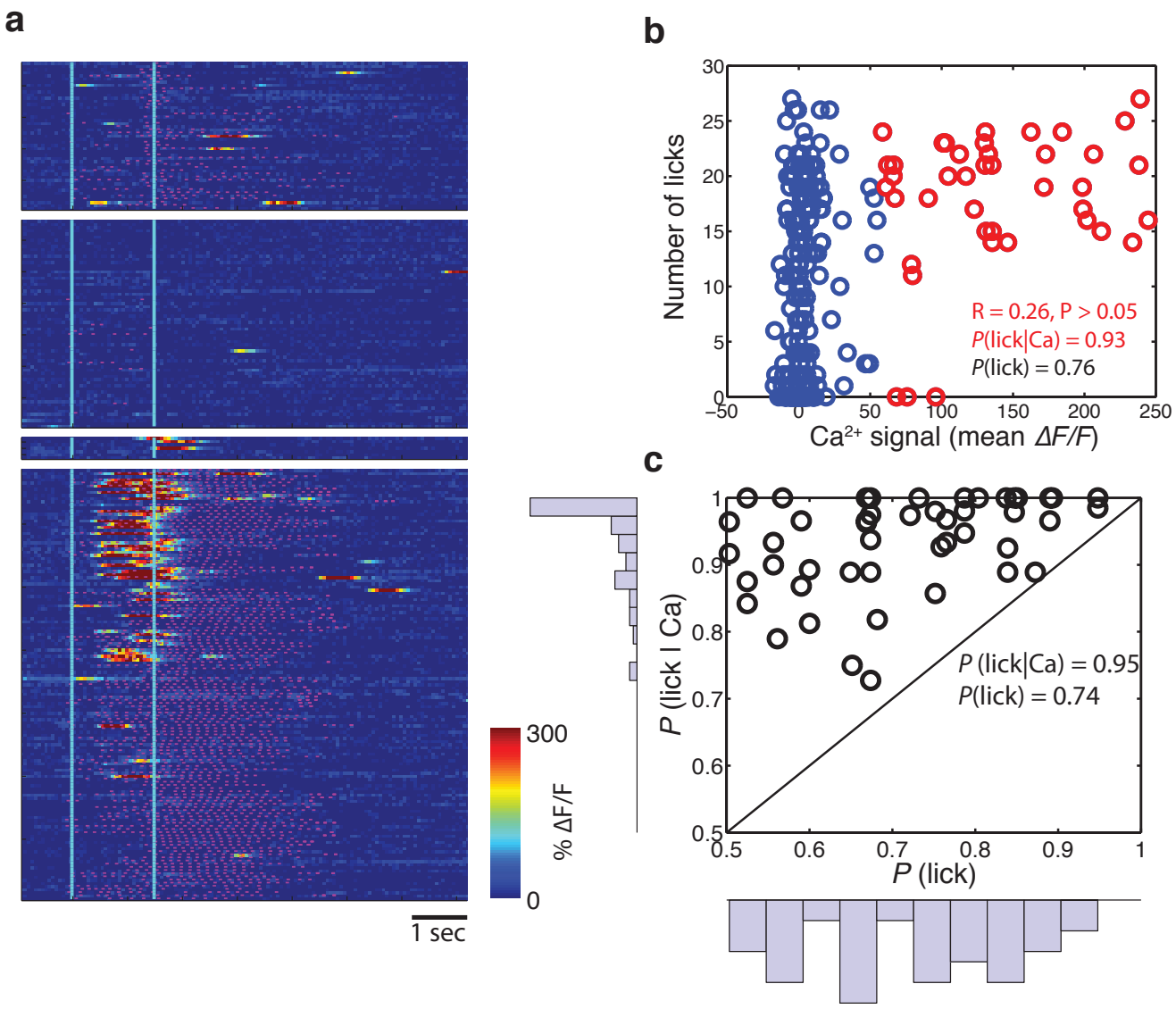

Supplementary Figure 11 | Dendritic Ca^{2+} signals and perceptual detection reported by licking. a, Color raster plot showing Ca^{2+} signals from one example dendritic branche. Lick times were marked by magenta ticks. **b,** Number of licks for each trial were plotted against mean Ca^{2+} signals. In trials showing large Ca^{2+} signals, no significant trial by trial correlation between Ca^{2+} signals and licking behavior (R = 0.26, P>0.05, for the current ROI; R = 0.011 ± 0.163 for 57 ROIs). Note that trials with strong Ca^{2+} signals (> 1 standard deviation, red symbols), show high probability of lick response [*P*(lick|Ca) = 0.93]. **c,** Population data of probability of lick response in trials with large Ca^{2+} signals (> 1 standard deviation; *P*(lick|Ca)) is significantly higher than probability of lick response over all trials [*P*(lick)].

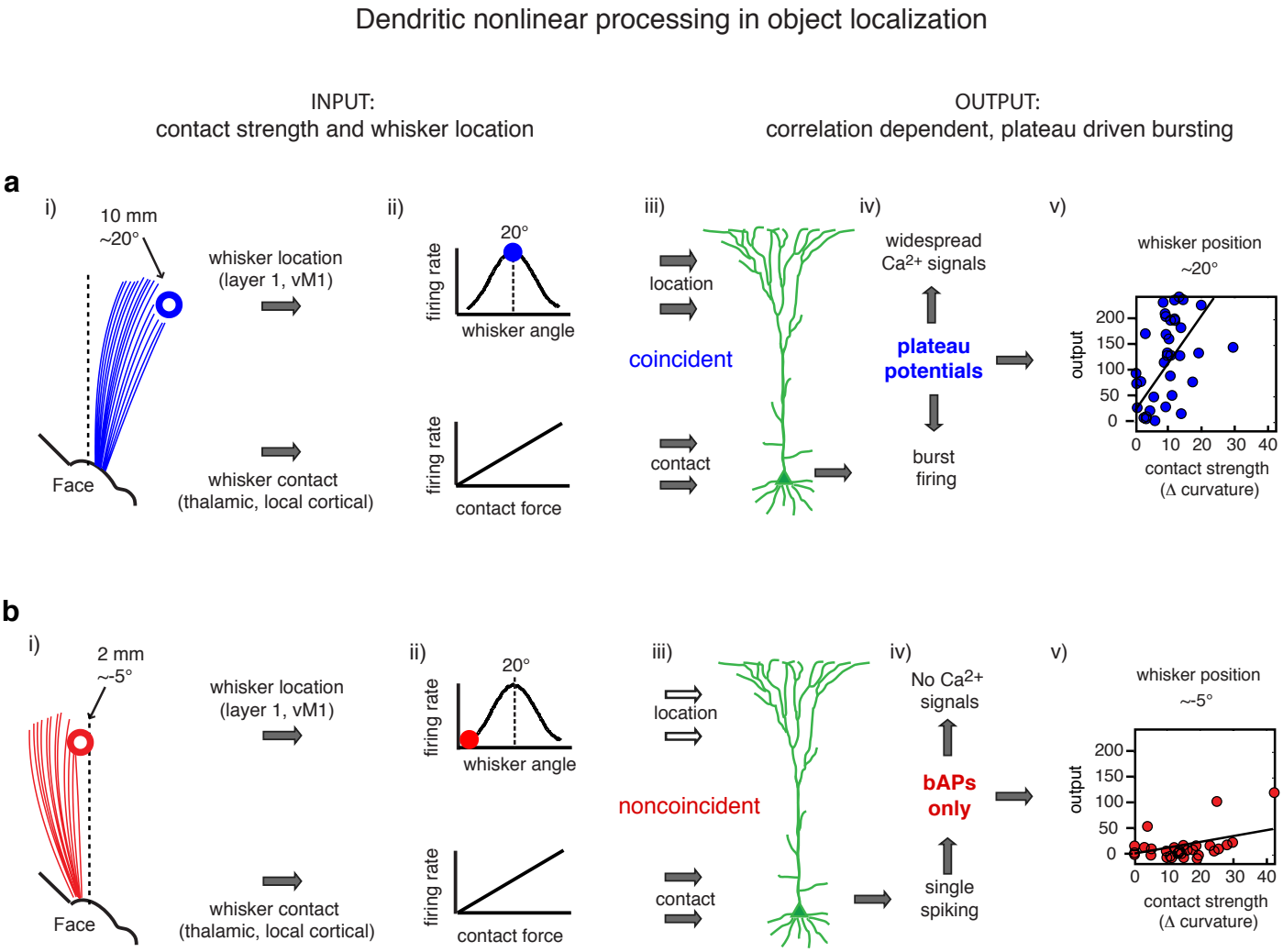

Supplementary Figure 12 | Proposed role of a dendritic nonlinearity in a behavioral relevant computation. a, Condition of coincident input (blue). i) schematic of whisking profile for object contact at 10 mm and whisker angles around 20°. ii) information representing whisker location could arrive through long-range cortico-cortical layer 1 inputs, among others, with vibrassal motor cortex as one potential source[3,23]. These inputs are shown here to have a preferred whisking feature that produces maximum firing rate around 20°. Whisker contact sensory input is delivered via thalamocortical and local barrel cortical inputs from layers 2/3 and 4[3] and is shown here to increase in amplitude with increased contact forces. Activity in these inputs could also posses some whisking related modulation. iii) whisker location dependent input is delivered to the dendritic tuft regions of layer 5 pyramidal neurons[3,23] while whisker contact sensory input is delivered to the perisomatic dendritic regions[3]. iv) coincident perisomatic and layer 1 inputs convert bAPs into multiple large amplitude, long duration regenerative plateau potentials in the distal dendritic region[4-7]. This nonlinear form of dendritic integration causes a large widespread Ca^{2+} influx throughout the apical tuft region and a burst of high frequency action potential output from the involved layer 5 neurons[21]. v) the plateau potential induced burst firing will enhance the slope of the stimulus-response relationship at the preferred whisking feature (20°) of the dominant layer 1 inputs. **b**, Noncoincident input (red). The panel layout is the same as **a**. Here whisker contact is in a different position (2 mm or ~-5°) and there is accordingly less layer 1 input arriving during the contact. With reduced amounts of layer 1 input, plateau potentials are not generated and the neuron remains in a low frequency single spiking mode. Without the large dendritic nonlinearity the slope of the stimulus-response curve is reduced.